nature structural & molecular biology

Intrinsic tethering activity of endosomal Rab proteins

Sheng-Ying Lo[1,2], Christopher L Brett[1,5], Rachael L Plemel[1], Marissa Vignali[3], Stanley Fields[3,4], Tamir Gonen[1,4,5] & Alexey J Merz[1]

Rab small G proteins control membrane trafficking events required for many processes including secretion, lipid metabolism, antigen presentation and growth factor signaling. Rabs recruit effectors that mediate diverse functions including vesicle tethering and fusion. However, many mechanistic questions about Rab-regulated vesicle tethering are unresolved. Using chemically defined reaction systems, we discovered that Vps21, a *Saccharomyces cerevisiae* ortholog of mammalian endosomal Rab5, functions in *trans* with itself and with at least two other endosomal Rabs to directly mediate GTP-dependent tethering. Vps21-mediated tethering was stringently and reversibly regulated by an upstream activator, Vps9, and an inhibitor, Gyp1, which were sufficient to drive dynamic cycles of tethering and detethering. These experiments reveal a previously undescribed mode of tethering by endocytic Rabs. In our working model, the intrinsic tethering capacity Vps21 operates in concert with conventional effectors and SNAREs to drive efficient docking and fusion.

Vesicle and organelle tethering are reversible recognition events that precede docking and bilayer fusion. Tethering also mediates transient contacts that allow materials such as lipids to be passed between organelles[1]. The most broadly deployed regulators of tethering are small G proteins of the Rab and Arf families[2,3]. These molecular switches, inactive when GDP bound, become activated upon GTP binding. Rabs are activated by guanosine nucleotide exchange factors (GEFs) that catalyze GDP expulsion to allow GTP binding, and they are inactivated by GTPase accelerating proteins (GAPs) that trigger the hydrolysis of GTP to GDP. Active GTP-bound Rabs recruit effector proteins that execute diverse functions including cytoskeletal transport, activation of lipid kinases, vesicle tethering and SNARE-mediated fusion.

Many Rabs and Rab effectors promote membrane tethering. However, tethering activity has generally been inferred from *in vivo* experiments or from assays using cell extracts or organelles. In these complex reaction systems, hundreds or thousands of molecular species are present; some directly mediate tethering whereas others act as upstream regulators that promote tethering but do not directly mediate it. For example, mammalian Rab5 regulates homotypic tethering and fusion of endosomes[4–9]. Rab5 promotes phosphatidylinositol-3-kinase activity that in turn generates binding sites for other molecules that mediate tethering, including the Rab5 effector EEA1 (refs. 10–12). EEA1 binding to 3-phosphoinositides is essential for its tethering activity *in vivo*. However, mutations in EEA1 that abrogate its high-affinity interactions with Rab5 do not interfere with EEA1 membrane association or endosome tethering. Instead, these mutations act downstream of tethering to block homotypic fusion[13]. Thus, although both Rab5 and EEA1 are unambiguously involved in endosome tethering, it remains uncertain whether Rab5 promotes tethering mainly by serving as a mechanical anchor for EEA1 (that is, Rab5 is part of the core tethering machinery), or whether the major role of Rab5 is to send instructive signals to other core tethering factors. There are similar uncertainties for the yeast Rab5 ortholog Vps21 and its effectors, and for the vast majority of other Rab-effector systems.

A central challenge in biochemistry is to reconstitute key biological processes using purified components, so as to define minimal reaction systems and explore their modes of action (for example, refs. 14–17). So far, only a handful of proteins have mediated tethering in chemically defined systems. These include GMAP-210, an effector of Arf1 at the Golgi[18], and HOPS, an effector of Ypt7 at the yeast vacuole[19–21]. For the vast majority of effectors currently known to promote tethering, it is uncertain whether their modes of action are mechanical or regulatory. Thus, the development of quantitative approaches to analyze the activities of putative tethering factors, especially factors that interact with Rabs, is a major goal in the field. While developing a general set of methods for this purpose, we discovered that Vps21 and other endosomal Rab proteins in *S. cerevisiae* not only bind classical effectors[22–27] but also undergo GTP-regulated Rab-Rab interactions that directly drive tethering *in vitro*, completely without effectors. These findings reveal a previously unknown intrinsic activity of endosomal Rabs in *S. cerevisiae*, and they suggest the presence of an additional layer of membrane-membrane recognition events in endosomal membrane traffic.

[1]Department of Biochemistry, University of Washington School of Medicine, Seattle, Washington, USA. [2]Department of Chemistry, University of Washington, Seattle, Washington, USA. [3]Department of Genome Sciences, University of Washington School of Medicine, Seattle, Washington, USA. [4]Howard Hughes Medical Institute, University of Washington School of Medicine, Seattle, Washington, USA. [5]Present addresses: Department of Biology, Concordia University, Montreal, Quebec, Canada (C.L.B.); and Janelia Farm Research Campus, Howard Hughes Medical Institute, Ashburn, Virginia, USA (T.G.). Correspondence should be addressed to A.J.M. (merza@uw.edu).

Received 30 May 2010; accepted 22 September 2011; published online 11 December 2011; doi:10.1038/nsmb.2162

RESULTS

Vps21-GTP tethers without Rab effectors

To directly and quantitatively evaluate the tethering capabilities and mechanisms of Rabs and effectors, we developed liposome-based *in vitro* systems. Native Rab proteins generally comprise a compact globular N-terminal GTP-binding domain and a C-terminal intrinsically disordered hypervariable domain of ~30 residues. Rabs associate with membranes through two geranylgeranyl lipids that are covalently attached to the extreme C terminus of the hypervariable domain. In our experiments, this lipid anchor was replaced by a C-terminal polyhistidine tag, which binds avidly to a synthetic lipid, Ni^{2+}-1,2-dioleoyl-*sn*-glycero-3-[*N*(5-amino-1-carboxypentyl)iminodiacetic acid)succinyl] (Ni^{2+}-NTA-DOGS). We prepared liposomes (~100-nm diameter) doped with Ni^{2+}-NTA-DOGS by extrusion, and then we decorated the liposomes with C-terminally His_{10}-tagged Rabs (**Fig. 1a**; see also ref. 28). We measured liposome tethering by quasielastic light scattering (QLS), which reports tethering in real time as an increase in effective particle diameter. The response of the QLS system was validated using mixtures of extruded liposomes of different diameters (see **Supplementary Methods**).

Unexpectedly, we observed robust GTP-dependent increases in effective particle diameter when liposomes were decorated with the *S. cerevisiae* endosomal Rab Vps21, without additional effector proteins (**Fig. 1b**). This particle size increase was nearly eliminated when Vps21 was preloaded with GDP rather than GTP, or when liposomes were decorated with the vacuolar-lysosomal Rab Ypt7. Because the particle size increases reported by QLS might have been due to either liposome tethering or membrane fusion, we examined aliquots from the liposome preparations by negative-stain transmission EM (TEM; **Fig. 1c**). TEM showed massive clusters of Vps21-GTP–decorated liposomes, but there was no evident size increase of individual liposomes within the clusters. Similarly, light microscopic observations of suspensions of fluorescently labeled liposomes in aqueous buffer (**Fig. 1d**) showed thousands of visible clusters in the presence of Vps21-GTP. After 40 min of incubation, the diffuse fluorescent background of individual, fast-diffusing Vps21-GTP liposomes was markedly depleted, indicating that most of the liposomes in the starting population were tethered within large clusters. These observations indicate that the Vps21-GTP liposome clusters seen by TEM formed in aqueous suspension, prior to deposition on the grid and negative staining. In sharp contrast to the tethering seen with Vps21-GTP, liposomes decorated with Vps21-GDP or liposomes decorated with Ypt7 bound to either GDP or GTP (**Fig. 1c**,**d**) did not form large clusters when examined by light microscopy or EM. Thus, three independent lines of evidence (QLS, TEM and fluorescence microscopy) indicate that Vps21-GTP drives efficient Rab-selective and GTP-dependent liposome tethering *in vitro*.

Tethering occurs at physiological Rab surface densities

To further characterize Vps21-mediated tethering, we titrated Rabs and lipids (**Fig. 2a**,**b** and **Supplementary Fig. 1**). The Ni^{2+} chelator lipid NTA-DOGS is anionic. The nitrilotriacetic acid (NTA) moiety has a net charge of –3, and it binds Ni^{2+} with 1:1 stoichiometry[29]. Ni^{2+}-NTA-DOGS-doped liposomes, like endocytic organelles, therefore have a net negative charge. Over a range of Ni^{2+}-NTA-DOGS concentrations, we observed strong tethering signals at Vps21-His_{10} surface densities of 1,500–7,000 μm^{-2}. In a comparable *in vitro* reconstitution of liposome tethering by another small G protein, Arf1, and its effector GMAP, tethering has been observed at Arf1 densities of 8,000–14,000 μm^{-2} and GMAP densities of 700–7,000 μm^{-2} (ref. 18). Notably, we found that tethering was highly responsive to the Vps21-GTP surface density (**Supplementary Fig. 1a**; Hill coefficient

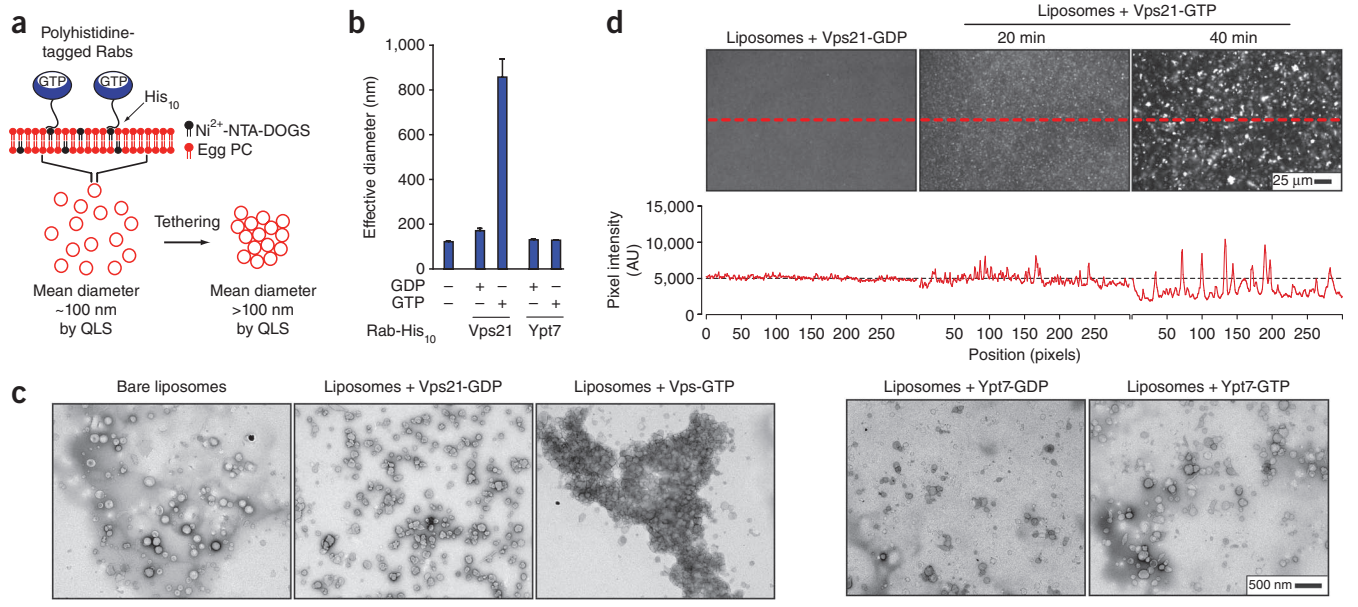

Figure 1 GTP-bound Vps21 tethers liposomes. (**a**) Experimental configuration. Full details are in Online Methods and **Supplementary Methods**. (**b**) Liposome particle size distributions were measured by QLS after 60-min incubation in the presence of the indicated Rab-His_{10} proteins, preloaded with GDP or GTP. Error bars indicate mean and s.e.m. for three independent experiments. (**c**) TEM images of negatively stained samples taken from experiment in **b**. (**d**) Liposomes were prepared as in **a**–**c**, except that fluorescent lipid was incorporated. Liposomes were incubated for 20 or 40 min, then a drop of the suspension was imaged by epifluorescence microscopy (200 ms exposure). Brightness and contrast adjustments are identical for the panels shown. Traces below the images show pixel intensities along the indicated dashed lines (AU, arbitrary units). Untethered liposomes are small and move rapidly and appear as diffuse fluorescence. As tethering proceeds, clusters grow in size and the fluorescent background markedly decreases indicating that most individual liposomes in the population have tethered. Liposomes with GDP- His_{10}-Vps21 are shown at 20 min incubation and were indistinguishable from those at 40 min incubation.

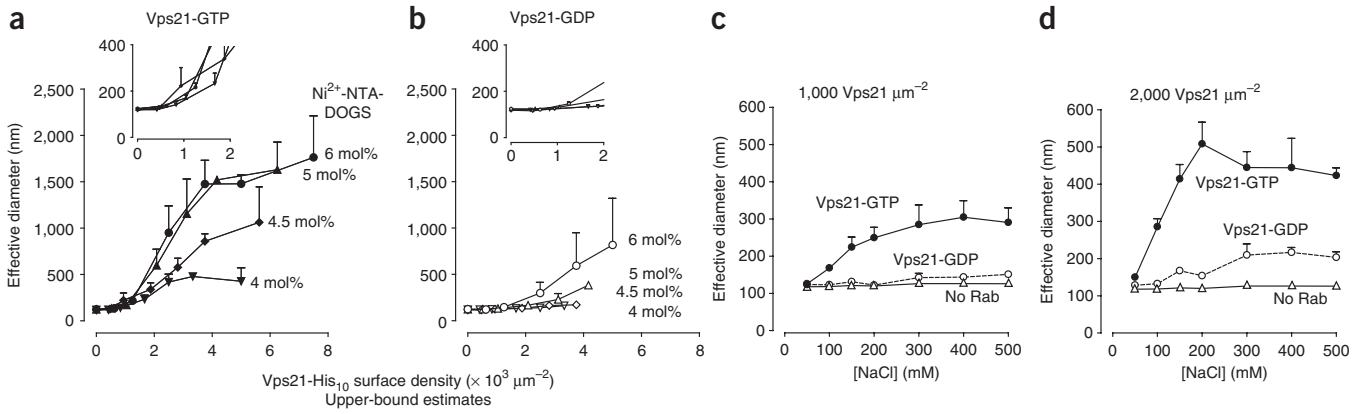

Figure 2 Vps21 surface density and tethering activity. (**a**,**b**) Liposome tethering, measured by QLS, was examined as a function of Vps21 membrane surface density. Vps21 was loaded with GTP (**a**) or GDP (**b**). Insets, onset of tethering at low Vps21 surface densities. Additional surface density data for Vps21 and Ypt7 are in **Supplementary Figure 1**. (**c**,**d**) To test effect of ionic strength, liposomes were decorated with Vps21-GDP or Vps21-GTP at two different surface densities, and tethering was monitored by QLS in buffers containing indicated salt concentrations. As in **a**,**b**, indicated Vps21 surface densities are upper-bound estimates. Data are mean and s.e.m. from three independent experiments.

≥3.5, 95% confidence limit). A simple interpretation of this dosage hypersensitivity is that tethering occurs through a cooperative mechanism that entails the concerted action of several Vps21-GTP complexes. Tethering was markedly lower when liposomes were decorated with inactive Vps21-GDP (**Fig. 2a**,**b** and **Supplementary Fig. 1b**). At very high ratios of Vps21-His_{10} to Ni^{2+}-NTA-DOGS, tethering was inhibited, probably through competitive inhibition by unbound Vps21-His_{10} (**Supplementary Fig. 1b**). With the vacuolar Rab Ypt7 (**Supplementary Fig. 1c**), we did not observe tethering at any concentration of Ni^{2+}-NTA-DOGS or Ypt7. This result is consistent with the demonstrated requirement for the HOPS effector complex in Ypt7-mediated tethering[19–21] and underscores the selectivity of Vps21-mediated tethering.

We next sought to determine whether Vps21-mediated tethering occurs within a physiologically relevant span of surface densities. To provide a criterion for the onset of tethering, we defined the critical surface density for tethering as the density of surface-bound Rab at which the effective particle diameter, measured by QLS, increases to twice the effective diameter of bare, untethered control liposomes. Nominally, at the critical surface density each liposome is on average tethered to one other liposome. The critical surface density for tethering by Vps21-GTP was ≤1,300 μm^{-2} (**Fig. 2a**,**b**, insets). This density corresponds to ~40 Vps21 molecules on the surface of an endosome of 100 nm diameter, or ~10 molecules on a 50-nm endosome. These are upper-bound estimates that assume that every Vps21 molecule in the assay system is both active and bound to a liposome. Although the Vps21 surface density on endosomes *in vivo* is unknown, estimates are available for the surface densities of two other Rabs. The density of Ypt7 on the *S. cerevisiae* vacuole is ~500 μm^{-2}, and the density of Rab3a on mammalian synaptic vesicles is ~1,950 μm^{-2} (**Supplementary Methods**; refs. 30–32). GTP-regulated tethering by Vps21 therefore occurs within the physiologically relevant range of Rab surface densities. Below this range detectable tethering does not occur, whereas above this range regulation by GTP binding is attenuated and tethering occurs constitutively.

To further characterize the interactions that drive Vps21-mediated tethering, we carried out QLS-based tethering assays across a range of salt concentrations (**Fig. 2c**,**d**). At subphysiological ionic strengths, tethering was potently inhibited. As the buffer ionic strength increased, the efficiency of tethering increased and then leveled off. Under all ionic conditions tested, we observed GTP selectivity, but the highest selectivity was at physiological ionic strength (150–200 mM NaCl). Inefficient tethering at low ionic strength could result from low shielding of the electrostatic repulsion between the negatively charged liposomes, or from decreased hydrophobic forces at protein interaction surfaces .

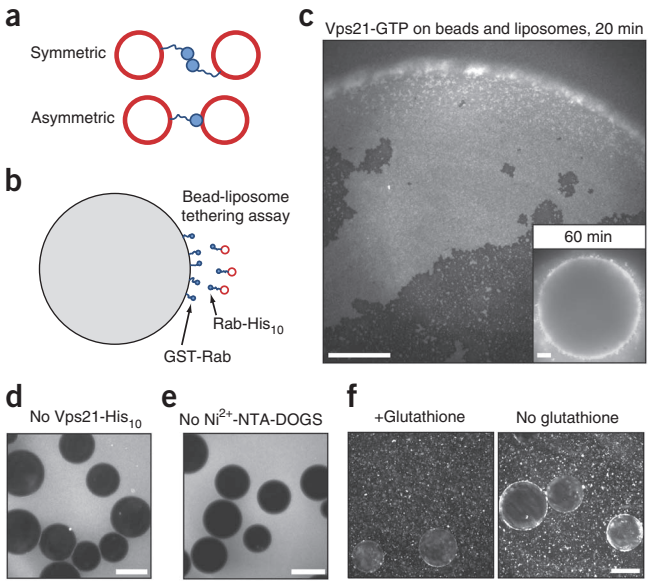

Figure 3 Vps21 interactions in *trans* are required for efficient tethering. (**a**) Schematic of two possible mechanisms of Rab-mediated tethering. (**b**) Schematic of bead-liposome tethering assay. (**c**) GTP-loaded GST–Vps21 beads were photographed after incubation for 20 or 60 min in presence of fluorescent liposomes containing 6 mol% Ni^{2+}-NTA-DOGS and GTP-loaded Vps21-His_{10}. Images are representative of nine independent experiments. (**d**) As in **c** (inset) but without GTP-loaded Vps21-His_{10}. (**e**) As in **c** (inset), but liposomes were prepared without Ni^{2+}-NTA-DOGS. (**f**) As in **c**, except that after 20 min incubation, 10 mM reduced glutathione was added (left), or buffer without glutathione was added (right). Samples were then incubated for 4 min more, then photographed. Scale bars, 15 μm (**c**) and 75 μm (**d**–**f**).

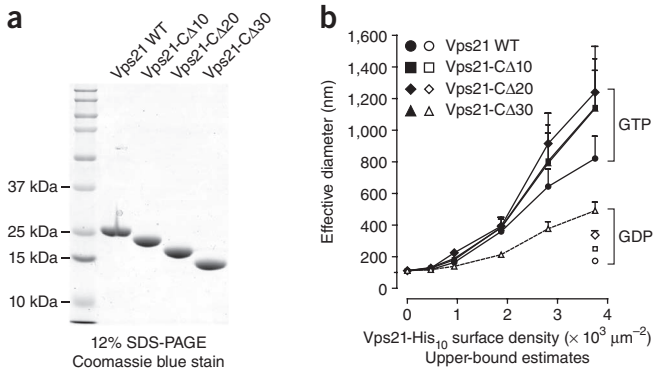

Figure 4 The Vps21 C-terminal linker is not required for tethering. (**a**) Vps21-His_{10} fusion proteins lacking last 10, 20 or 30 residues of the Vps21 C-terminal linker were prepared. Purified proteins (5 μg) were analyzed by SDS-PAGE. (**b**) Liposomes bearing these proteins were assayed by QLS for the ability to drive tethering over indicated range of surface densities. Each construct was loaded with either GTP (filled symbols) or GDP (open symbols). Liposomes contained 4.5 mol% Ni^{2+}-NTA-DOGS. Error bars indicate mean and s.e.m. from four independent experiments.

Rab-Rab interactions in *trans* drive efficient tethering

In principle, Vps21-mediated tethering might occur through either a symmetric or an asymmetric mechanism (**Fig. 3a**). In the symmetric mechanism, Vps21 anchored to opposite membranes would dimerize or oligomerize in *trans* to drive tethering. This mechanism depends on protein-protein contacts. In the asymmetric mechanism, a single Vps21 molecule anchored to one vesicle would undergo GTP-triggered direct binding to the lipids of the opposite vesicle. It is also possible that both classes of mechanisms could contribute to Vps21-mediated tethering.

To assess these hypotheses, we used a bead-liposome assay that allows the components on two tethering surfaces to be varied independently (**Fig. 3b**). A similar system has been used to probe the binding of nucleoporin proteins to phospholipid bilayers[33]. Large (~100 μm) glutathione-agarose beads were decorated with glutathione-*S*-transferase (GST)-Rab fusion proteins. The beads were mixed with a suspension of small (~100 nm) fluorescent liposomes with Rab-His_{10} proteins. Tethering of the liposomes to the beads was evident by epifluorescence microscopy as a fluorescent halo at the beads' surfaces (**Fig. 3c**). Using this assay, we found that efficient tethering requires GTP-bound Vps21 anchored to both partner surfaces. Tethering did not occur without Vps21-His_{10} (**Fig. 3d**) or when Vps21-His_{10} attachment to liposomes was prevented by omission of Ni^{2+}-NTA-DOGS (**Fig. 3e**). Similarly, tethered liposomes fell off of the beads when GST-Vps21 was dissociated from the beads by soluble glutathione (**Fig. 3f**). Tethering was also abrogated when Ypt7 replaced Vps21 on either the beads or the liposomes (**Supplementary Fig. 2a**). The inability of bead-bound GST-Vps21 to tether either bare liposomes or liposomes bearing Ypt7 is evidence against asymmetric tethering mechanisms in which GTP binding triggers a Vps21 interaction solely by interacting with the *trans* bilayer. Moreover, substitution of GDP for GTP on GST-Vps21 (beads), on Vps21-His_{10} (liposomes) or on both substantially attenuated tethering (**Supplementary Fig. 2b**). Thus for optimal tethering, Rabs on both partner surfaces must be activated. This result mirrors the symmetrical requirement for activated Rab5-GTP in homotypic docking and fusion of mammalian endosomes[9]. In sum, these results support models in which symmetrical Vps21-Vps21 contacts in *trans* are required for tethering. However, we have so far not detected Vps21 dimerization or oligomerization in solution-based assays (for example, **Supplementary Fig. 3**). Together, these results suggest that restraining Vps21 on a two-dimensional membrane surface may increase avidity to drive tethering. It is also possible, however, that affinity components derived from both protein-membrane and protein-protein interactions are required for efficient tethering (see Discussion).

The Vps21 C-terminal linker is not required for tethering

Native Vps21, like most other Rabs, consists of a compact N-terminal GTP-binding domain that attaches to membranes through a disordered ~30-residue C-terminal linker bearing a doubly geranylgeranylated membrane anchor at its extreme C terminus. To ascertain whether the Vps21 C-terminal linker contributes to tethering, we prepared a set of Vps21-His_{10} mutants with truncated C-terminal linkers (**Fig. 4a**) and evaluated the capacity of these mutants to promote liposome tethering in the QLS assay (**Fig. 4b**). Each of the mutants mediated GTP-dependent tethering with efficiency equivalent to or greater than that of full-length Vps21. Thus, the C-terminal linker domain is not directly involved in the tethering reaction.

Vps21 interacts with other endosomal Rabs to drive tethering

Taken together, our biochemical studies suggest that efficient Vps21-mediated tethering involves a protein-protein interaction, GTP-stimulated Vps21-Vps21 association in *trans*. Unbiased yeast two-hybrid screens provided additional evidence that Vps21 interacts with itself and also with other endosomal Rabs.

In a separate project, we sought to identify new Rab-interacting proteins by carrying out systematic yeast two-hybrid screens. In all our yeast two-hybrid experiments, we used low-copy rather than high-copy vectors, and we carried out the read-out growth assays with 3-aminotriazole, conditions that almost eliminate false positives[34,35]. Using the 11 *S. cerevisiae* Rabs as baits, we interrogated ordered prey arrays containing >5,000 *S. cerevisiae* open reading frames. More than 65,000 crosses yielded ~340 candidate interactions. Among these interactions were many expected Rab interactions with known Rab effectors (ref. 36 and unpublished results), and there were interactions we expected with Rab-specific chaperones, including Rab GDP dissociation inhibitor, Rab escort protein and Yif and Yip proteins (**Supplementary Table 1**). To our surprise, however, the screen repeatedly identified homotypic and heterotypic Rab-Rab interactions among endosomal Rabs. In our initial screens, we detected the Rab5 orthologs Vps21, Ypt52, Ypt53 and Ypt10, the

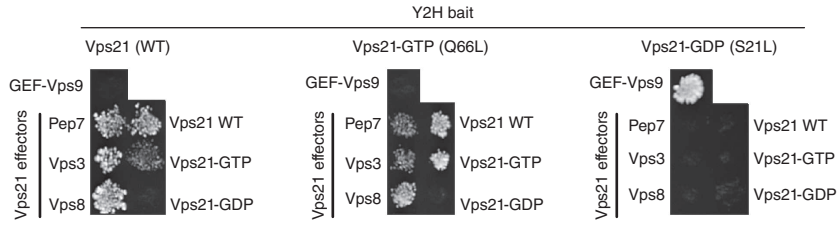

Figure 5 Vps21-GTP interacts with known effectors and with itself in yeast two-hybrid assays. A positive interaction in the yeast two-hybrid assay is indicated by yeast colony growth on medium lacking tryptophan, leucine and histidine, and supplemented with 1.5 mM 3-aminotriazole. The Vps21 effectors Vac1 (also known as Pep7), Vps3 and Vps8 are positive controls for interaction selectivity with Vps21-GTP, whereas Vps9 is a control for interaction selectivity with Vps21-GDP.

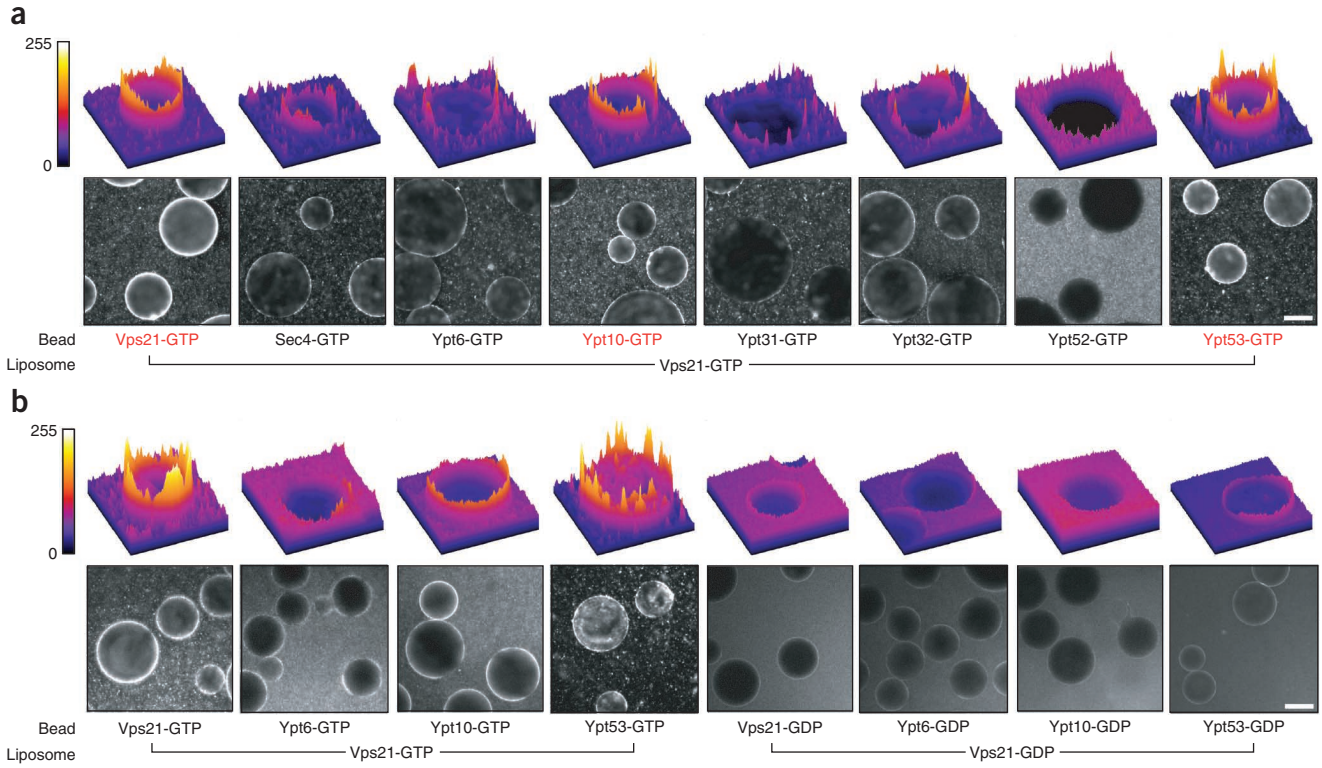

Figure 6 Vps21 interacts with Ypt53 and Ypt10 to drive GTP-dependent heterotypic tethering. (**a**) Heterotypic Rab-Rab tethering was assayed as in **Figure 3** except that beads were decorated with various GTP-loaded GST-Rab fusion proteins, as indicated. Bottom, representative fields of beads under epifluorescence illumination. Top, fluorescence intensity profile plots of representative beads. (**b**) Assays were done as in **a**, except that the Rabs were preloaded with either GTP or GDP. Ypt6, which does not interact with Vps21, was a negative control. Scale bars, 75 μm.

Rab6 ortholog Ypt6 and the Rab 7 ortholog Ypt7 in heterotypic and homotypic Rab-Rab interactions (**Supplementary Table 1**). Moreover, physical interactions among Vps21, Ypt52 and Ypt53 have been independently reported in high-throughput proteomic surveys[37], and mammalian Rab5 isoforms have been reported to undergo GTP-dependent dimerization[38].

In focused yeast two-hybrid assays using independently constructed prey vectors, most of the interactions detected in the high-throughput screens were reproduced and extended (**Supplementary Table 2**), with the Vps21 self-interaction yielding a robust signal (**Fig. 5** and **Supplementary Tables 2** and **3**). Notably, Vps21 interactions with itself and with other Rabs were restricted to wild-type Vps21 and the dominant-active mutant Vps21 Q66L. Moreover, these yeast two-hybrid interactions were similar in signal strength and nucleotide selectivity to Vps21 interactions with its three known effectors, Vps3, Vps8 and Vac1 (refs. 22,23,27,39). We did not observe Rab-Rab or Rab-effector interactions when either bait or prey was the GDP-biased mutant Vps21 S21L. As we expected, the Vps21 S21L mutant robustly interacted with the Vps21 nucleotide exchange factor Vps9 (ref. 40) but not with Vps21 effector proteins. These yeast two-hybrid data provide evidence for GTP-dependent interactions among multiple yeast endosomal Rab proteins and buttress our biochemical results showing that Vps21-mediated tethering is driven by homotypic interactions between activated, membrane-anchored Vps21 molecules.

To ascertain whether heterotypic interactions between Vps21 and other Rabs can drive tethering, as suggested by the yeast two-hybrid results, we used the bead-liposome assay (**Fig. 6**). Beads decorated with various GST-Rab fusions were mixed with fluorescent liposomes bearing Vps21-His_{10}. In these assays (**Fig. 6a**), tethering was mediated by Vps21-GTP with Ypt53 or Ypt10, two other Rabs of the endosomal Rab5 group[41]. In each case, substitution of GDP for GTP abrogated tethering (**Fig. 6b**). Several other Rabs including another Rab5 paralog, Ypt52, did not mediate heterotypic tethering with Vps21 (**Fig. 6a**). Because Vps21-GTP liposomes can interact with one another, there may be competition between Vps21 on the liposomes and the Rabs shown on the beads, reducing the apparent heterotypic tethering signal between Vps21 and any Rabs that Vps21 binds with lower affinity than the self-interaction. This type of competition, if it did occur, would make the bead-liposome assay more stringent and could prevent detection of weaker Rab-Rab tethers. Taken together, the yeast two-hybrid experiments and tethering assays reveal a network of GTP-stimulated homotypic and heterotypic interactions among endosomal Rabs. A subset of these pairs can mediate GTP-dependent tethering *in vitro*.

Regulation of tethering by Vps21 GEF and GAP

Regulation and reversibility are hallmarks of Rab-controlled tethering reactions. Upstream regulators of Vps21 include Vps9, a GEF[40], and Gyp1, a GAP[42,43]. We therefore evaluated whether Vps9 and the Gyp1 catalytic core $Gyp1_{TBC}$ can control Vps21-mediated tethering. Using solution-phase assays, we first verified the catalytic activities of our Vps9 and $Gyp1_{TBC}$ preparations (**Supplementary Fig. 4**). We then investigated whether Vps9 could stimulate tethering by promoting nucleotide exchange. Liposomes bearing Vps21-GDP, monitored by QLS, tethered when both GTP and Vps9 were added to the reactions (**Fig. 7a**). Next, we examined the reversibility of tethering. When added to pretethered liposomes bearing Vps21-GTP, the GAP $Gyp1_{TBC}$ efficiently reversed tethering, again with dose-dependent kinetics at concentrations as low as 10 nM (**Fig. 7b**). The catalytically

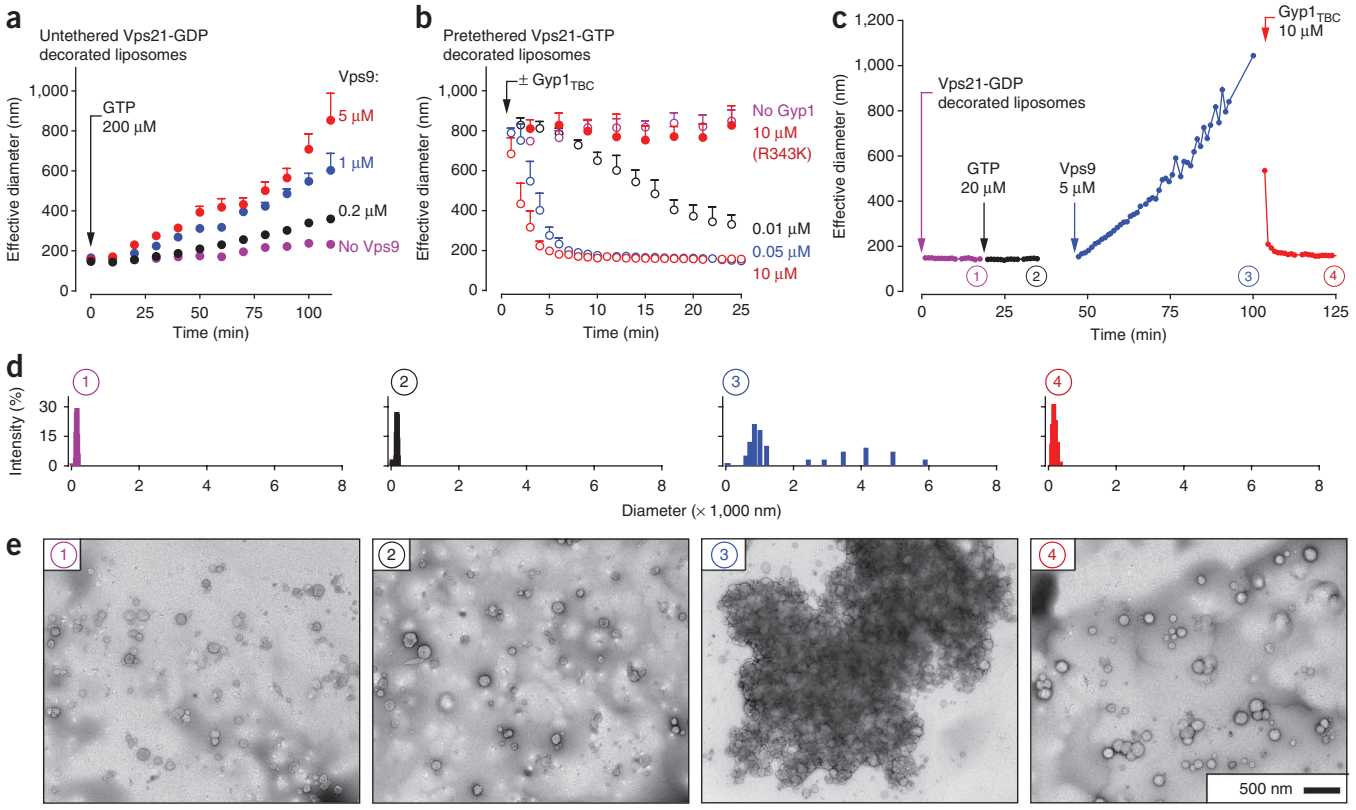

Figure 7 Regulation and reversibility of Vps21-mediated liposome tethering. (**a**) GEF-stimulated tethering. Tethering by GDP-loaded Vps21-decorated liposomes was measured by QLS after addition of 0.2 mM GTP and varying concentrations of Vps9. Data are mean and s.e.m.; data points from three independent experiments were binned into 10-min intervals. (**b**) GAP-mediated reversal of tethering. GTP-loaded Vps21-decorated liposome tethering was measured by QLS after addition of $Gyp1_{TBC}$ or $Gyp1_{TBC\text{-}R343K}$. Error bars indicate mean and s.e.m.; data from three independent experiments were binned into 2-min intervals. (**c**) Regulated cycle of tethering and detethering. Vps21-mediated liposome tethering, measured by QLS, was examined during sequential addition of 20 μM GTP, 5 μM Vps9 and 10 μM $Gyp1_{TBC}$. Data are representative of three independent experiments. (**d**) Histograms of Vps21-decorated liposome size distributions, derived from QLS, at time points indicated in **c**. (**e**) TEM images of negatively stained samples withdrawn at indicated time points from experiment analyzed in **c**,**d**.

inactive mutant[43] $Gyp1_{TBC\text{-}R343K}$ had no effect on tethering even when added at 10 μM. GTP hydrolysis is therefore essential for the $Gyp1_{TBC}$-mediated disassembly of Vps21-GTP-mediated tethers (**Fig. 7b**).

Finally, in sequential-addition experiments, we reconstituted a complete cycle of regulated tethering and detethering (**Fig. 7c–e**). Liposomes decorated with Vps21-GDP were monitored by QLS (**Fig. 7c**). Addition of GTP alone had no effect, but subsequent Vps9 addition initiated an immediate and steady increase in tethering. Addition of $Gyp1_{TBC}$ rapidly reversed Vps9-stimulated tethering. QLS-derived particle size distributions (**Fig. 7d**) and TEM analysis of aliquots taken from the same reactions (**Fig. 7e**) verified that Vps9 and $Gyp1_{TBC}$ can drive complete cycles of tethering and detethering. Thus, Vps21-mediated tethering without effectors is Rab-selective, regulated by GTP, completely reversible and strictly controlled by upstream regulators.

DISCUSSION

Small G proteins orchestrate many biological processes, generally by acting through specialized effectors. Nevertheless, some small G proteins have intrinsic capabilities that complement or enhance the activities of their effectors. In vesicle formation, for example, activated Arf1 and Sar1 recruit the COPI and COPII coat complexes. However, the N-terminal domains of these small G proteins also interact directly with membranes to generate positive membrane curvature[44,45]. Here we have shown that like Arf1 and Sar1, Vps21 and some other yeast endosomal Rab proteins have both intrinsic and effector-mediated capabilities: they can dimerize or oligomerize in *trans* to tether membranes in a stringently GTP-dependent, tightly regulated and fully reversible reaction. In our working model, this intrinsic tethering

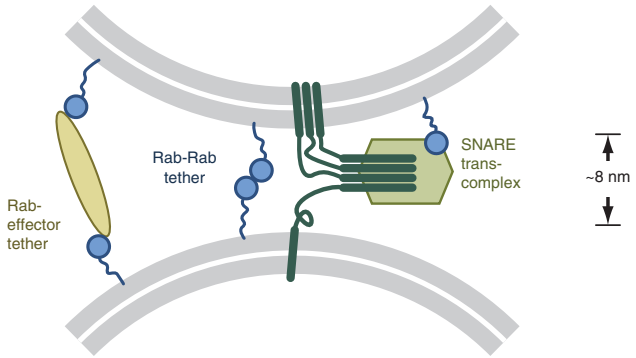

Figure 8 Model for Rab-Rab driven tethering in endosome docking and fusion. In this working model, three representative Rab functions are shown: classical effector-mediated tethering, Rab-Rab tethering and coordination of *trans*-SNARE complex assembly by a Rab-mediated recruitment of a SNARE-binding regulator. Together, these mechanisms could in principle coordinate an ordered tethering, docking and fusion sequence.

mechanism would cooperate with classical Rab-effector mechanisms to promote membrane tethering, docking and fusion (**Fig. 8**).

There are previous reports of Rab-Rab interactions. Rab5a, Rab5b and Rab5c, the closest mammalian orthologs of Vps21, have been detected in homotypic and heterotypic dimers by yeast two-hybrid assay, and Rab5b dimerizes *in vitro* and *in vivo* in an apparently GTP-dependent manner[38]. Moreover, in structural studies, the GDP-bound forms of Rab9 and Rab11a form crystallographic dimers[46–48]. So far, all Rabs reported to dimerize operate within endocytic trafficking pathways. These interactions are consistent with our results for yeast endocytic Rabs, raising the possibility that dimerization of endocytic Rabs is a general theme. The potential for complex regulation of tethering through Rab-Rab interactions is underscored by our identification of Rab pairs that show heterotypic interactions in yeast two-hybrid experiments and by our demonstration that a subset of these Rab pairs mediates heterotypic tethering in the liposome-bead assay. Similarly, Arf1, another small G protein, dimerizes during vesicle formation[49]. However, Arf1 does not mediate membrane tethering except in the presence of an effector[18]. Dimerization of Arf1 therefore seems restricted to *cis* rather than *trans* interactions.

Our biochemical and biophysical results demonstrate that Vps21 and some other endosomal Rabs have an intrinsic ability to tether membranes *in vitro*. Nevertheless, questions about the detailed mechanism of this tethering activity and its biological consequences remain. Although our results indicate that Vps21-Vps21 interactions are involved in tethering, we have so far not detected Vps21 dimerization or oligomerization in solution-phase assays using techniques including size-exclusion chromatography and multiangle light scattering. These findings raise the possibility that Vps21 dimerization is augmented by uncharacterized interactions between Vps21-GTP and the membrane. A requirement for both protein-protein and protein-membrane interactions in GTP-triggered tethering would be reminiscent of the requirement for interactions between synaptotagmin and SNARE proteins, and between synaptotagmin and lipids, in Ca^{2+}-riggered fusion[50].

The relative *in vivo* contributions to yeast endosome tethering by intrinsic Vps21 activity and by more conventional Vps21-effector mechanisms are not yet characterized, and they remain to be analyzed *in vivo*. Such experiments will require the isolation of Vps21 mutants that interact with the normal complement of Rab chaperones, upstream regulators and effectors, but which lack intrinsic tethering capacity. We are currently conducting genetic screens to identify and characterize mutant alleles with these properties.

If Rabs recruit specialized effectors, some of which are tethers, what is the function of Rab-Rab tethering? We suggest two possibilities. First, there is some redundancy among Rabs and effectors. For example, the yeast protein Vps8 is the only effector of Vps21 currently known to promote tethering *in vivo*. Vps8 is also needed for biosynthetic trafficking of carboxypeptidase Y to the vacuole. Notably, however, functional defects caused by Vps8 deletion are efficiently suppressed by Vps21 overproduction[24]. Conversely, Vps8 overexpression without Vps21 does not seem to mediate tethering[26]. These results support working models in which Vps8 and Vps21 normally act in concert, whereas without Vps8, an elevated level of secondary Vps21-mediated tethering is sufficient to support endolysosomal traffic. This secondary tethering activity could be mediated by Vps21-Vps21 interactions, by Vps21 interactions with another effector, or by some combination of these activities.

A second possible function for Rab-Rab tethering is suggested by the fact that Rab-Rab tethers probably operate at shorter range than classical effector-based tethers. Known and presumed tethers often assume extended structures that are presumed to allow vesicle capture and tethering over substantial distances (tens of nanometers). By contrast, Rab-Rab tethering must occur over shorter distances. Most Rabs attach to the membrane through a ~35-residue C-terminal disordered linker, which is doubly prenylated at its end. Our results show that the Vps21 linker is not needed for tethering (**Fig. 4**), but it probably influences the distance between tethered membranes. Because disordered polypeptides act as Brownian springs, Rabs probably interact in *trans* between membranes separated by ≤10 nm (**Fig. 8** and **Supplementary Methods**). Similarly, kinetically stable *trans*-SNARE complexes assemble only once docked membranes approach to within ~8 nm (refs. 51,52), raising the possibility of a 'handoff' mechanism whereby effector-mediated tethers promote Rab-Rab tethering, which, in turn, stably hold the membranes close enough to promote the initiation of SNARE zippering and fusion (**Fig. 8**). In the cases of Rab5 and Vps21, SNARE pairing is regulated by Vps45, a Sec1-Munc18 family protein recruited to the fusion site by Rab5 effector rabenosyn-5 or its yeast ortholog Vac1 (refs. 22,23,53,54). Finally, we speculate that Rab-Rab tethering might have emerged early in eukaryotic evolution, preceding more complex systems in which effectors contributed additional capabilities, including coordination of multiple small G proteins[2,55], tethering over longer distances[56], coupling of Rab activation to vesicle coat dynamics[57] and *trans*-SNARE complex assembly and membrane fusion[21,52,58].

METHODS

Methods and any associated references are available in the online version of the paper at http://www.nature.com/nsmb/.

Note: Supplementary information is available on the Nature Structural & Molecular Biology website.

ACKNOWLEDGMENTS

We thank P. Brennwald and J. Taraska for helpful discussion and D. Baker and R. Koga for assistance with multiangle light scattering experiments. High-throughput screening and support of M.V. was through the Yeast Resource Center (US National Institutes of Health (NIH) P41 RR11823). S.L. was supported in part by University of Washington Nanotechnology Integrative Graduate Education and Research Traineeship award (US National Science Foundation DGE-0504573). We thank the Murdock Charitable Trust and the Washington Research Foundation for generous support of our electron cryomicroscopy laboratory. T.G. was a Howard Hughes Medical Institute early career scientist and S.F. is a Howard Hughes Medical Institute investigator. This work was supported by NIH grant GM077349 and research scholar grant 10-026-01-CSM from the American Cancer Society.

AUTHOR CONTRIBUTIONS

S.Y.L. and A.J.M. conceived the project. S.Y.L. developed and validated the QLS-based tethering system; expressed, purified and characterized proteins; prepared liposomes and carried out and interpreted all QLS tethering experiments. C.L.B. and A.J.M. conceived and C.L.B. and S.Y.L. implemented the fluorescence microscopy-based tethering assays. T.G. did the E M. S.F. and M.V. developed the high-throughput yeast two-hybrid technology, and R.L.P. and M.V. executed and interpreted yeast two-hybrid screens and assays. S.Y.L. and A.J.M. wrote the paper.

COMPETING FINANCIAL INTERESTS

The authors declare no competing financial interests.

Published online at http://www.nature.com/nsmb/.
Reprints and permissions information is available online at http://www.nature.com/reprints/index.html.

1. Kornmann, B. *et al.* An ER-mitochondria tethering complex revealed by a synthetic biology screen. *Science* **325**, 477–481 (2009).
2. Grosshans, B.L., Ortiz, D. & Novick, P. Rabs and their effectors: achieving specificity in membrane traffic. *Proc. Natl. Acad. Sci. USA* **103**, 11821–11827 (2006).
3. Barr, F.A. Rab GTPase function in Golgi trafficking. *Semin. Cell Dev. Biol.* **20**, 780–783 (2009).
4. Singer-Kruger, B. *et al.* Role of three Rab5-like GTPases, Ypt51p, Ypt52p, and Ypt53p, in the endocytic and vacuolar protein sorting pathways of yeast. *J. Cell Biol.* **125**, 283–298 (1994).

5. Horazdovsky, B.F., Busch, G.R. & Emr, S.D. *VPS21* encodes a Rab5-like GTP binding protein that is required for the sorting of yeast vacuolar proteins. *EMBO J.* **13**, 1297–1309 (1994).
6. Gerrard, S.R., Bryant, N.J. & Stevens, T.H. *VPS21* controls entry of endocytosed and biosynthetic proteins into the yeast prevacuolar compartment. *Mol. Biol. Cell* **11**, 613–626 (2000).
7. Gorvel, J.P., Chavrier, P., Zerial, M. & Gruenberg, J. Rab5 controls early endosome fusion *in vitro*. *Cell* **64**, 915–925 (1991).
8. Bucci, C. *et al.* Co-operative regulation of endocytosis by three Rab5 isoforms. *FEBS Lett.* **366**, 65–71 (1995).
9. Barbieri, M.A. *et al.* Evidence for a symmetrical requirement for Rab5-GTP in *in vitro* endosome-endosome fusion. *J. Biol. Chem.* **273**, 25850–25855 (1998).
10. Simonsen, A. *et al.* EEA1 links PI(3)K function to Rab5 regulation of endosome fusion. *Nature* **394**, 494–498 (1998).
11. Christoforidis, S., McBride, H.M., Burgoyne, R.D. & Zerial, M. The Rab5 effector EEA1 is a core component of endosome docking. *Nature* **397**, 621–625 (1999).
12. Christoforidis, S. *et al.* Phosphatidylinositol-3-OH kinases are Rab5 effectors. *Nat. Cell Biol.* **1**, 249–252 (1999).
13. Lawe, D.C. *et al.* Sequential roles for phosphatidylinositol 3-phosphate and Rab5 in tethering and fusion of early endosomes via their interaction with EEA1. *J. Biol. Chem.* **277**, 8611–8617 (2002).
14. Davie, E.W. A brief historical review of the waterfall/cascade of blood coagulation. *J. Biol. Chem.* **278**, 50819–50832 (2003).
15. Weber, T. *et al.* SNAREpins: minimal machinery for membrane fusion. *Cell* **92**, 759–772 (1998).
16. Antonny, B., Madden, D., Hamamoto, S., Orci, L. & Schekman, R. Dynamics of the COPII coat with GTP and stable analogues. *Nat. Cell Biol.* **3**, 531–537 (2001).
17. Wollert, T. & Hurley, J.H. Molecular mechanism of multivesicular body biogenesis by ESCRT complexes. *Nature* **464**, 864–869 (2010).
18. Drin, G., Morello, V., Casella, J.F., Gounon, P. & Antonny, B. Asymmetric tethering of flat and curved lipid membranes by a golgin. *Science* **320**, 670–673 (2008).
19. Hickey, C.M. & Wickner, W. HOPS initiates vacuole docking by tethering membranes prior to trans-SNARE complex assembly. *Mol. Biol. Cell* **21**, 2297–2305 (2010).
20. Hickey, C.M., Stroupe, C. & Wickner, W. The major role of the Rab Ypt7p in vacuole fusion is supporting HOPS membrane association. *J. Biol. Chem.* **284**, 16118–16125 (2009).
21. Stroupe, C., Hickey, C.M., Mima, J., Burfeind, A.S. & Wickner, W. Minimal membrane docking requirements revealed by reconstitution of Rab GTPase-dependent membrane fusion from purified components. *Proc. Natl. Acad. Sci. USA* **106**, 17626–17633 (2009).
22. Peterson, M.R., Burd, C.G. & Emr, S.D. Vac1p coordinates Rab and phosphatidylinositol 3-kinase signaling in Vps45p-dependent vesicle docking/fusion at the endosome. *Curr. Biol.* **9**, 159–162 (1999).
23. Tall, G.G., Hama, H., DeWald, D.B. & Horazdovsky, B.F. The phosphatidylinositol 3-phosphate binding protein Vac1p interacts with a Rab GTPase and a Sec1p homologue to facilitate vesicle-mediated vacuolar protein sorting. *Mol. Biol. Cell* **10**, 1873–1889 (1999).
24. Horazdovsky, B.F., Cowles, C.R., Mustol, P., Holmes, M. & Emr, S.D. A novel RING finger protein, Vps8p, functionally interacts with the small GTPase, Vps21p, to facilitate soluble vacuolar protein localization. *J. Biol. Chem.* **271**, 33607–33615 (1996).
25. Peplowska, K., Markgraf, D.F., Ostrowicz, C.W., Bange, G. & Ungermann, C. The CORVET tethering complex interacts with the yeast Rab5 homolog Vps21 and is involved in endo-lysosomal biogenesis. *Dev. Cell* **12**, 739–750 (2007).
26. Markgraf, D.F. *et al.* The CORVET subunit Vps8 cooperates with the Rab5 homolog Vps21 to induce clustering of late endosomal compartments. *Mol. Biol. Cell* **20**, 5276–5289 (2009).
27. Plemel, R.L. *et al.* Subunit organization and Rab interactions of Vps-C protein complexes that control endolysosomal membrane traffic. *Mol. Biol. Cell* **22**, 1353–1363 (2011).
28. Gureasko, J. *et al.* Membrane-dependent signal integration by the Ras activator Son of sevenless. *Nat. Struct. Mol. Biol.* **15**, 452–461 (2008).
29. Hochuli, E., Dobeli, H. & Schacher, A. New metal chelate adsorbent selective for proteins and peptides containing neighbouring histidine residues. *J. Chromatogr. A* **411**, 177–184 (1987).
30. Wang, L., Seeley, E.S., Wickner, W. & Merz, A.J. Vacuole fusion at a ring of vertex docking sites leaves membrane fragments within the organelle. *Cell* **108**, 357–369 (2002).
31. Ghaemmaghami, S. *et al.* Global analysis of protein expression in yeast. *Nature* **425**, 737–741 (2003).
32. Takamori, S. *et al.* Molecular anatomy of a trafficking organelle. *Cell* **127**, 831–846 (2006).
33. Patel, S.S. & Rexach, M.F. Discovering novel interactions at the nuclear pore complex using bead halo: a rapid method for detecting molecular interactions of high and low affinity at equilibrium. *Mol. Cell. Proteomics* **7**, 121–131 (2008).
34. Braun, P. *et al.* An experimentally derived confidence score for binary protein-protein interactions. *Nat. Methods* **6**, 91–97 (2009).
35. Chen, Y.C., Rajagopala, S.V., Stellberger, T. & Uetz, P. Exhaustive benchmarking of the yeast two-hybrid system. *Nat. Methods* **7**, 667–668 author reply 668 (2010).
36. Brett, C.L. *et al.* Efficient termination of vacuolar Rab GTPase signaling requires coordinated action by a GAP and a protein kinase. *J. Cell Biol.* **182**, 1141–1151 (2008).
37. Ho, Y. *et al.* Systematic identification of protein complexes in *Saccharomyces cerevisiae* by mass spectrometry. *Nature* **415**, 180–183 (2002).
38. Daitoku, H., Isida, J., Fujiwara, K., Nakajima, T. & Fukamizu, A. Dimerization of small GTPase Rab5. *Int. J. Mol. Med.* **8**, 397–404 (2001).
39. Pawelec, A., Arsic, J. & Kolling, R. Mapping of Vps21 and HOPS binding sites in Vps8 and effect of binding site mutants on endocytic trafficking. *Eukaryot. Cell* **9**, 602–610 (2010).
40. Hama, H., Tall, G.G. & Horazdovsky, B.F. Vps9p is a guanine nucleotide exchange factor involved in vesicle-mediated vacuolar protein transport. *J. Biol. Chem.* **274**, 15284–15291 (1999).
41. Buvelot Frei, S. *et al.* Bioinformatic and comparative localization of Rab proteins reveals functional insights into the uncharacterized GTPases Ypt10p and Ypt11p. *Mol. Cell. Biol.* **26**, 7299–7317 (2006).
42. Du, L.L., Collins, R.N. & Novick, P.J. Identification of a Sec4p GTPase-activating protein (GAP) as a novel member of a Rab GAP family. *J. Biol. Chem.* **273**, 3253–3256 (1998).
43. Pan, X., Eathiraj, S., Munson, M. & Lambright, D.G. TBC-domain GAPs for Rab GTPases accelerate GTP hydrolysis by a dual-finger mechanism. *Nature* **442**, 303–306 (2006).
44. Lee, M.C. *et al.* Sar1p N-terminal helix initiates membrane curvature and completes the fission of a COPII vesicle. *Cell* **122**, 605–617 (2005).
45. Pucadyil, T.J. & Schmid, S.L. Conserved functions of membrane active GTPases in coated vesicle formation. *Science* **325**, 1217–1220 (2009).
46. Wittmann, J.G. & Rudolph, M.G. Crystal structure of Rab9 complexed to GDP reveals a dimer with an active conformation of switch II. *FEBS Lett.* **568**, 23–29 (2004).
47. Pasqualato, S. *et al.* The structural GDP/GTP cycle of Rab11 reveals a novel interface involved in the dynamics of recycling endosomes. *J. Biol. Chem.* **279**, 11480–11488 (2004).
48. Scapin, S.M. *et al.* The crystal structure of the small GTPase Rab11b reveals critical differences relative to the Rab11a isoform. *J. Struct. Biol.* **154**, 260–268 (2006).
49. Beck, R. *et al.* Membrane curvature induced by Arf1-GTP is essential for vesicle formation. *Proc. Natl. Acad. Sci. USA* **105**, 11731–11736 (2008).
50. Chapman, E.R. How does synaptotagmin trigger neurotransmitter release? *Annu. Rev. Biochem.* **77**, 615–641 (2008).
51. Li, F. *et al.* Energetics and dynamics of SNAREpin folding across lipid bilayers. *Nat. Struct. Mol. Biol.* **14**, 890–896 (2007).
52. Schwartz, M.L. & Merz, A.J. Capture and release of partially zipped trans-SNARE complexes on intact organelles. *J. Cell Biol.* **185**, 535–549 (2009).
53. Nielsen, E. *et al.* Rabenosyn-5, a novel Rab5 effector, is complexed with hVPS45 and recruited to endosomes through a FYVE finger domain. *J. Cell Biol.* **151**, 601–612 (2000).
54. Furgason, M.L. *et al.* The N-terminal peptide of the syntaxin Tlg2p modulates binding of its closed conformation to Vps45p. *Proc. Natl. Acad. Sci. USA* **106**, 14303–14308 (2009).
55. Sinka, R., Gillingham, A.K., Kondylis, V. & Munro, S. Golgi coiled-coil proteins contain multiple binding sites for Rab family G proteins. *J. Cell Biol.* **183**, 607–615 (2008).
56. Hayes, G.L. *et al.* Multiple Rab GTPase binding sites in GCC185 suggest a model for vesicle tethering at the trans-Golgi. *Mol. Biol. Cell* **20**, 209–217 (2009).
57. Angers, C.G. & Merz, A.J. New links between vesicle coats and Rab-mediated vesicle targeting. *Semin. Cell Dev. Biol.* **22**, 18–26 (2011).
58. Ohya, T. *et al.* Reconstitution of Rab- and SNARE-dependent membrane fusion by synthetic endosomes. *Nature* **459**, 1091–1097 (2009).

ONLINE METHODS

Proteins. See **Supplementary Methods** for detailed descriptions of protein expression construct, expression and purification.

Liposomes. A 2.5-mg quantity of lipids consisting of egg phosphatidylcholine (PC) and Ni^{2+}-NTA-DOGS dissolved in chloroform (Avanti Polar Lipids) were mixed, dried under an argon stream and placed under vacuum overnight. For assays requiring fluorescent liposomes, 0.4 mol% Texas Red DPPE (Invitrogen) was incorporated into the lipid mixture. Lipid films were hydrated in liposome reaction buffer (20 mM HEPES-NaOH, pH 7.5, 150 mM NaCl, 1 mM $MgCl_2$ and 2 mM 2-mercaptoethanol) to 2.5 mg ml^{-1} before extrusion through a 0.1 μm polycarbonate filter (Avanti Polar Lipids). To change the ionic strength of the liposome environment, liposomes were prepared in liposome reaction buffer at the indicated NaCl concentrations.

Quasielastic light scattering tethering assay. In general, samples were prepared by incubating 100 μl of liposomes with 20 μl nucleotide-loaded Rab-His_{10} at 24.5 °C for 1 h, then diluted to 1 ml for QLS measurement. See **Supplementary Methods** for detailed information on QLS. Nucleotide-loaded Rab-His_{10} protein was prepared by incubating 4–5 mg ml^{-1} Rab-His_{10} with a 30-fold molar excess of guanine nucleotide and 5 mM EDTA for 1 h at 25–27 °C in 20 mM HEPES-NaOH, pH 7.5, 150 mM NaCl and 1 mM DTT. Nucleotide exchange was terminated with 10 mM $MgCl_2$ on ice for 15 min and free nucleotide was removed by size exclusion using a Micro Bio-Spin column (Bio-Rad) pre-equilibrated with liposome reaction buffer at the indicated NaCl concentration.

Rab membrane density was altered by incubating liposomes at varying Rab to Ni^{2+}-NTA-DOGS molar ratios (**Supplementary Table 4**). Except as indicated, liposomes contained 4.5 mol% Ni^{2+}-NTA-DOGS and were incubated with 20 μl of Rab-His_{10} at a molar ratio of 0.067:1 Rab/Ni^{2+}-NTA-DOGS, yielding a surface density of ≤3,750 Vps21-His_{10} μm^{-2}. For GEF experiments, Vps9 was added to 200 μl of liposomes preincubated with GDP-bound Vps21-His_{10} and diluted to 640 μl for QLS measurement. GTP (10 μl) was added to initiate tethering. For GAP experiments, 200 μl of liposomes preincubated with GTP-loaded Vps21-His_{10} was diluted to 550 μl for QLS measurement. $Gyp1_{TBC}$ or $Gyp1_{TBC\text{-}R343K}$ (100 μl) was added to initiate disassembly of liposome clusters. For the reconstitution of a full tethering cycle, 400 μl liposomes were preincubated with GDP-bound Vps21-His_{10}. The mixture was diluted to 640 μl for QLS measurements, and GTP, Vps9 and $Gyp1_{TBC}$ were subsequently added, in order, to final volumes of 650 μl, 700 μl and 850 μl. The concentrations of GTP, Vps9 and $Gyp1_{TBC}$ were maintained at 20 μM, 5 μM and 10 μM, respectively, throughout the sequential-addition experiment.

Fluorescent tethering assay and bead-liposome tethering assay. GST-Rab-coupled glutathione–Sepharose 4B beads (GE Healthcare) were prepared as described[27,36] except that an equal volume of *Escherichia coli* lysate expressing untagged $Gyp1_{TBC}$ was mixed with the Rab-expressing cell lysate to drive Rab conversion into the GDP-bound state. Nucleotide loading of Rabs was done by incubating GST-Rab beads in loading buffer (50 mM HEPES-NaOH, pH 7.8, 100 mM NaCl, 5 mM 2-mercaptoethanol, 5 mM EDTA and 500 μM guanine nucleotide) for 1 h at 24.5 °C. An equal volume of quenching buffer (50 mM HEPES-NaOH, pH 7.8, 100 mM NaCl, 5 mM 2-mercaptoethanol and 10 mM $MgCl_2$) was then added to each reaction and incubated for an additional 15 min. Nucleotide-loaded GST-Rab beads were then washed twice with reaction buffer (20 mM HEPES-NaOH, pH 7.4, 125 mM NaCl, 5 mM 2-mercaptoethanol and 5 mM $MgCl_2$). Fluorescent liposome tethering reactions or bead-liposome tethering reactions were prepared on ice by mixing 50 μl reaction buffer and 40 μl fluorescent liposome suspension with or without 50 μl of packed, nucleotide-loaded GST-Rab beads. Nucleotide-loaded Rab-His_{10} (6 μg) was then added to initiate tethering. The upper-bound density of Vps21-His_{10} on liposomes used for the bead assay was ≤4,700 Vps21-His_{10} μm^{-2}. Reactions were brought to 24.5 °C, incubated for 20, 40 or 60 min, then imaged.

Micrographs were acquired using a microscope (IX71; Olympus) equipped with an electron-multiplying charge-coupled device (iXon; Andor). Epifluorescence illumination was done by green and blue light-emitting diodes (>350-mW output) coupled to the microscope's back aperture by a multimode optical fiber and driven by custom electronics. Objective lenses were UPlanApo (0.40 numerical aperture (NA), 10×) or PlanApoN (1.45 NA, 60×). The microscope and camera were driven by iQ software (version 6.0.3.62; Andor), and micrographs were processed using ImageJ (version 1.36b; NIH) and Photoshop (version 8.0; Adobe). For display, images were sharpened by applying unsharp masking.

Electron microscopy. For negative-stain EM, samples were stained with 0.75% (w/v) uranyl formate. Images were collected using a 100 kV transmission electron microscope (Morgagni M268, FEI) equipped with a Gatan bottom mount 4k × 2k charge-coupled device camera. Images were recorded at either 4,400× or 8,900× magnification at the specimen level.

Yeast two-hybrid assays. Genome-wide two-hybrid analysis was done as described[13] in collaboration with the University of Washington Yeast Resource Center. Parent strains and plasmids were obtained from the Yeast Resource Center. Two-hybrid constructs were cloned individually into haploid tester strains using gap repair and homologous recombination. Prey domains were cloned into the plasmid pOAD and transformed into the yeast strain PJ69-4a. Bait domains were cloned into pOBD2 and transformed into PJ69-4α. Clonal isolates were obtained and verified by PCR. Sequencing was done using dideoxy chain termination.

Focused interaction tests were done by mating bait and prey haploid strains in 96-well plates, which were then pinned to YPD plates supplemented with adenine using a 48-spoke inoculating manifold. The mating plates were grown at 30 °C overnight before selecting diploids by replica plating onto medium supplemented with adenine but lacking tryptophan and leucine. Diploid colonies were grown at 30 °C for 2 d, then replica plated to medium supplemented with adenine and 1.5 mM 3-amino-1,2,4-triazole but lacking tryptophan, leucine and histidine. Plates were scored for growth after 5 d at 30 °C.

doi:10.1038/nsmb.2162